Simulative assessment of non-linear interference generation within disaggregated optical line systems

Research Article | Vol. 3, No. 12 / 15 December 2020 / OSA Continuum 3378

Simulative assessment of non-linear interference generation within disaggregated optical line systems

ELLIOT LONDON,[1,*] EMANUELE VIRGILLITO,[1] ANDREA D'AMICO,[1] ANTONIO NAPOLI,[2] AND VITTORIO CURRI[1]

[1] *Department of Electronics and Telecommunications, Politecnico di Torino, Corso Duca degli Abruzzi 24, 10129 Torino, Italy*
[2] *Infinera, St.-Martin-Straβe 76, 81541 München, Germany*
[*] *elliot.london@polito.it*

Abstract: Lightpaths within optical line systems (OLS)s that deploy coherent optical technologies are mainly impaired by two additive Gaussian disturbances: the amplified spontaneous emission (ASE) noise from the optical amplifiers and the non-linear interference (NLI) from fiber propagation, together with some amount of phase noise, typically compensated for by the carrier phase estimator module within the digital signal processing (DSP) unit. The main obstacle in accurately modelling the physical layer of a disaggregated optical network arises from the spatially-coherent and spectrally-aggregated general behavior of the NLI generation. Within this paper, we perform an accurate split-step Fourier method (SSFM) physical layer simulation campaign over a wide range of fiber chromatic dispersion values that range from 2 to 16.7 ps / (nm·km) and channel symbol rates from 32 GBd to 85 GBd. For all the explored scenarios, we first show that the NLI generation in an OLS can be spectrally disaggregated in a practical manner by considering a superposition of self-channel (SC) and cross-channel (XC) NLI components only. Secondly, by considering the span-by-span generalized signal-to-noise ratio (GSNR) deterioration, we show that the XC-NLI accumulation components can also be considered as spatially disaggregated, leaving the SC-NLI as the only spatial coherency contribution. Consequently, by appropriately managing these coherent NLI contributions, we find that it is possible to produce a conservative physical layer model that is both spectrally and spatially disaggregated.

1. Introduction

Within the past decade there has been a marked increase in optical network capacities and transmission rates [1,2]. This trend is expected to accelerate in the wake of ever-growing end user demands, corresponding to the increased popularity of cloud-based services, forays into consumer software with large data streaming requirements, such as virtual- and augmented-reality [3–5] and the implementation and development of 5G-enabled services [6,7]. Furthermore, network operators that deal with fast-adapting optical systems utilizing virtualized software environments have requirements that are shifting optical network structures towards disaggregation, where optical line system (OLS) components are controlled by different operators [8,9] in a possibly multi-vendor and inter-operable scenario [10].

This shift towards disaggregation has been spurred by an increase in OLS flexibility requirements [11], requiring OLS components to be considered independently [12], which may prevent the lightpath (LP) routing history from being fully known. Aside from complicating wavelength assignment and transmission standardization, this approach also causes the history of LPs to become either partially or wholly obscured due to communication between different operators and systems not yet being standardized. This consideration leads to both *spatial* and *spectral*

#410333 https://doi.org/10.1364/OSAC.410333
Journal © 2020 Received 17 Sep 2020; revised 29 Oct 2020; accepted 6 Nov 2020; published 1 Dec 2020

OSA CONTINUUM

disaggregation being required, with the former needed to overcome the lack of LP history knowledge and the latter being a request to enable alien wavelength management, network slicing down to the physical layer and to simplify multi-band transmission management. From a physical layer modelling perspective this is a key issue as, in general, the non-linear interference (NLI) generation behaves coherently [13–15] with respect to propagation distance and thus depends upon the LP history. However, as the the NLI generation is a non-linear phenomenon, in principle it is not spectrally disaggregated.

The mathematical modelling of the NLI has experienced several efforts in recent history. In [16,17] the NLI was modelled by manipulating the non-linear Schrödinger equation (NLSE) in the frequency domain as a Four-Wave Mixing (FWM)-like noise, approaching the problem from a spectrally aggregated perspective. Theoretical approaches to the calculation of NLI are still being developed – we highlight in particular [18], which presents an analytical solution to the NLSE using a regular perturbation. In [19–22] the self-channel (SC) and cross-channel (XC) components of the NLI are treated separately, considering the NLI generation in the time domain and observing collisions among pulses. In the widely-used Gaussian noise (GN) model [13,16,23] the NLI is considered as an additive Gaussian noise with incoherent spatial accumulation. This model has been generalized for frequency and space-dependent gain and losses in [24]. Following a spectrally and spatially aggregated approach, accurate mathematical models for NLI generation have also been proposed and effectively tested [25] with excellent results, also for closed-form expressions, but generally require large computational times. Although aggregated models have been shown to be accurate and conservative for current, widespread optical network configurations [26,27], the coherent contribution to the total NLI increases with the symbol rate, reducing their accuracy [15] and hampering the efforts of network controllers in predicting the quality of transmission (QoT) degradation.

Furthermore, even if accurate, such approaches are not adequate for the control and management of a spatially and spectrally disaggregated network [28], because the entire LP history and full spectral information are often needed as inputs. To achieve this, the NLI contribution on a given channel under test (CUT) must be considered as independently generated; both on a fiber-by-fiber basis (spatially disaggregated) and as the superposition of the independent effects generated by each co-propagating channel (spectrally disaggregated). Regarding the single-channel non-linear effect (SC-NLI); a greater QoT impairment on the LP is produced as symbol rates increase, which progresses in line with advancements in commercial equipment [1]. A method to conservatively consider the SC-NLI in a disaggregated environment has been proposed in [15]. Regarding the NLI contributions generated by co-propagating wavelength-division multiplexed (WDM) channels, i.e. the cross-channel non-linear effects (XC-NLI), a Gaussian noise mathematical model has been proposed in [14]. It has been demonstrated that a spectrally and spatially disaggregated approach to the XC-NLI generation loses accuracy as cross-channel correlation lengths increase, occurring when the accumulated dispersion, fiber length or symbol rate decreases [25,29], however an assessment on the limits of this approach has not yet clearly presented. In this paper, we aim at defining such limits, observing the accumulation of SC- and XC-NLI components by accurate split-step Fourier method (SSFM) simulations, within a wide scenario of dispersion values, symbol rates and WDM grid values.

The remainder of the manuscript is organized as follows: In Sec. 2 we revise the principle of the disaggregated network abstraction. In Sec. 3 we provide a detailed description of the simulation setup, considering a point-to-point OLS made of periodically and transparently amplified fiber spans. The simulation campaign explored values of dispersion from 2 up to 16.7 ps / (nm·km) and symbol rates, R_s, from 32 GBd up to 85 GBd. Additionally, different WDM flex-grid scenarios are analyzed to test $R_s/\Delta f$ ratio values of 0.64 and 0.85. We performed both pump-and-probe (P&P) and full spectral load (full-spectrum) simulations to investigate the spectral disaggregation and calculated the NLI contribution after each fiber span to test the spatial disaggregation hypothesis.

OSA CONTINUUM

In Sec. 4 we show that the total NLI contribution (SC-NLI + XC-NLI) of an OLS transmitting under full spectral load may be obtained through a superposition of P&P simulations, highlighting that NLI generation can be practically considered as spectrally disaggregated for most commercial applications. Following this, in Sec. 5 we observe the accumulation of the XC-NLI, showing that it can be considered as spatially disaggregated for all the analyzed cases, expanding upon the results of [14]. In Sec. 6 we remark that an accurate abstraction of optical fiber transmission is possible for fully disaggregated networks following the approach presented in [28], at the very least for the configuration ranges considered within this work. Finally, in Sec. 7 we recap the main findings of our study. With the proposed approach being valid down to a dispersion of 2 ps / (nm·km), we highlight that in reference to a multi-band OLS over ITU-T G.652D fiber the spectrally and spatially disaggregated approach to NLI generation can be effectively applied for the L+C+S+E bands and partially on the O-band, for fiber span lengths of tens of kilometers.

2. Physical layer abstraction in a disaggregated optical network

Estimating QoT degradation in an OLS is commonly performed by calculating the generalized signal-to-noise ratio (GSNR) degradation, which can be used as a unique figure of merit for the QoT of a LP [27]. This assumption holds when each LP can be modelled as an additive Gaussian noise channel, i.e. when the amplified spontaneous emission (ASE) noise from the amplifiers, the NLI from fiber propagation and any other potential impairment on the CUT can be treated as additive Gaussian noise sources [13]. This is pertinent for modern optical systems, where the non-linear phase noise (NLPN) and transmitter phase noise are significantly compensated for by adequate carrier phase estimation (CPE) algorithms in digital-signal-processing (DSP)-based receivers [30,31]. This approach has been extensively validated: we highlight in particular for multi-vendor scenarios [27] and for QPSK, 8-QAM and 16-QAM transceivers [32]. For an OLS composed of N_s fiber spans, indexed by n, the total GSNR at the end of the last fiber span is given by:

$$\mathrm{GSNR} = \left(\sum_{n=1}^{N_s} \mathrm{GSNR}_n^{-1} \right)^{-1} . \tag{1}$$

The GSNR of Eq. 1 may be fully separated into its two contributions: the OSNR considering the ASE noise of the optical amplifiers and the non-linear SNR ($\mathrm{SNR_{NL}}$) accounting for the NLI-generated noise sources. A fully disaggregated optical network may conceivably be composed of a variety of different fiber types and transponder types, each giving varying contributions to the total GSNR. Considering first the nature of the ASE noise, this contribution is modelled by individually characterizing each amplifier within the OLS, meaning that its accumulation is fully separable from the NLI contributions and causes no major issues when modelling the physical layer of a disaggregated optical network. On the other hand, the NLI disturbance generally behaves coherently, meaning that the NLI generated at a given fiber span is linked to the history of the propagated signal along the LP and is dependent upon several system and transmission parameters such as symbol rate, channel frequency spacing and launch powers of all active WDM channels. This limitation would be a significant issue when the LP history cannot be fully known. As a consequence, we focus only upon the NLI noise within this work and how to estimate it independently of the LP history.

Starting from a spectrally disaggregated approach, it is possible to decompose the NLI into its two main constituents: the XC-NLI and the SC-NLI effects. The XC effects are generated by a given channel interfering with all other channels, including the cross-phase modulation (XPM) and the FWM effects. The SC effects coincide with the self-phase modulation (SPM), which arises from the NLI generated by a channel interfering with itself. The XC-NLI component due to FWM [25] is a spectrally *aggregated* disturbance that depends upon the non-linear crosstalk generated by three channels. However, in [25,29] it has been shown that the FWM

OSA CONTINUUM

component is negligible in most practical scenarios, meaning that for all practical purposes the XC-NLI coincides with the XPM. The XPM contribution to the NLI is well approximated as a statistical effect for a wide range of use cases, serving to be both incoherent, local and able to be analyzed from a fully disaggregated perspective [14,33]. In contrast, the SPM provides a coherent contribution, being a non-local effect that hinders a disaggregated approach unless steps are taken to quantify its asymptotic maximum after a given number of spans [15]. It has been shown that the SPM and XPM effects can be separated [14,25,29], for all realistic use cases [14,33], even if an evaluation of the application boundaries have not yet been performed. This implies that it may be possible to formulate a scenario including both spectral and spatial disaggregation, allowing a fully disaggregated model of an optical network to be realized, starting from the physical layer.

Applying the concept of spectral separability, it is possible to calculate the total amount of NLI power, P_{NLI}, generated on a single CUT as the sum of the individual channel contributions, $P_{\mathrm{NLI,k}}$, with k as the channel index:

$$P_{\mathrm{NLI}} = \underbrace{P_{\mathrm{NLI},0}}_{SPM} + \underbrace{\sum_{k\neq 0} P_{\mathrm{NLI},k}}_{XPM} , \tag{2}$$

where the first ($k = 0$) term refers to the SPM of the CUT upon itself and the second ($k \neq 0$) summation term encloses the XPM contribution generated by all the other channels, usually referred to as the XPM pumps. The corresponding total $\mathrm{SNR_{NL}}$ of the CUT is thus given by $\mathrm{SNR_{NL}} = P_{ch}/P_{\mathrm{NLI}}$, with P_{ch} as the CUT launch power.

Furthermore, assuming spatial separability of both the SPM and XPM terms allows the total P_{NLI} to also be summed on a span-by-span basis. Therefore, the total $\mathrm{SNR_{NL}}$ for each channel k, after n spans can be calculated as the reciprocal sum of the inverse non-linear SNR degradation contributions $\mathrm{SNR_{NL},}_{k,n}$:

$$\mathrm{SNR_{NL}} = \left[\sum_{n=1}^{N_s}\left(\frac{1}{\mathrm{SNR_{NL},}_{n,0}} + \sum_{k\neq 0}\frac{1}{\mathrm{SNR_{NL},}_{n,k}}\right)\right]^{-1} . \tag{3}$$

Given the total $\mathrm{SNR_{NL}}$ and the intensity of each disaggregated $\mathrm{SNR_{NL},}_{k,n}$ contribution, Eq. 3 enables an assessment of the spectral and spatial disaggregation hypotheses.

3. Simulation campaign

We conducted an extensive SSFM simulation campaign, using our internally developed, MATLAB based software framework [34], comparing two distinct simulation scenarios, denoted as the *full-spectrum* and *superimposed* cases. The full-spectrum scenario is the propagation of a multi-channel WDM signal, representing the target system under investigation. Conversely, the superimposed case performs separate P&P simulations considering the propagation of 2 channels per simulation; the CUT (the probe) and another channel acting as the XPM pump, taken from the WDM comb simulated in the corresponding multi-channel simulation. We highlight that the full-spectrum simulations include all possible propagation effects, whereas the P&P simulations are aimed at capturing only the XPM generated independently by each pump. Eq. 3 is then used to obtain the superposition of each individual P&P simulation result. The superimposed estimation of the $\mathrm{SNR_{NL}}$ is then compared to the $\mathrm{SNR_{NL}}$ of the full-spectrum simulation. As an example, the normalized power spectral density (PSD) observed via simulation after propagation through 20 fiber spans is presented in Fig. 1(a-b), showing the spectra of a single P&P and of the full-spectrum case. Outlines of the simulation set-up and of the constellation are visible in Fig. 2(a) and Fig. 2(b), respectively.

Our software framework is able to generate a dense WDM comb signal, originating from a DSP-based coherent transceiver. The CUT is always polarization multiplexed-quadrature phase shift

OSA CONTINUUM

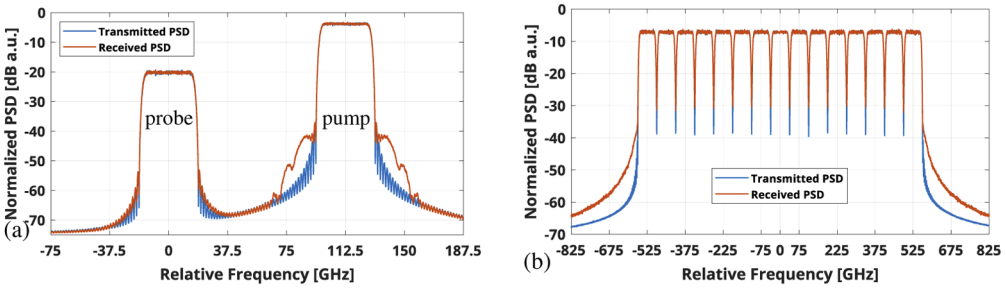

Fig. 1. The normalized PSD observed before (blue) and after (red) propagation through 20 fiber spans, in a scenario where $R_s = 32\,\text{GBd}$, $\Delta f = 50\,\text{GHz}$ and $D = 2\,\text{ps}/(\text{nm}\cdot\text{km})$, for: (a) a single P&P simulation and (b) a full-spectrum simulation.

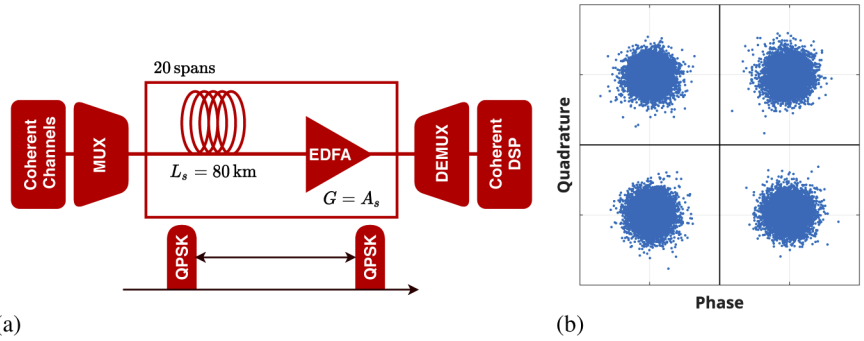

Fig. 2. (a), The simulation set-up and (b), the constellation of the QPSK modulated probe in a P&P simulation.

keying (PM-QPSK) modulated. Each quadrature of the two polarization components is generated using an independent pseudo-random binary sequence (PRBS) with a 15-th degree polynomial. Concerning the interfering channels (the XPM pumps), we investigate two distinct scenarios – first they are simulated as dual polarization QPSK modulated without any pre-distortion in order to represent the transmission over an OLS considered as a standalone system. Secondly, the interfering channels are simulated as Gaussian modulated signals in order to consider a more general case where the line is a subsystem of a network with interfering channels that have each travelled various distances. The channels within an OLS can be considered as Gaussian modulated if a sufficient amount of dispersion has been accumulated during propagation over these distances [35]. Each channel is then up-sampled and shaped with a raised cosine-filter with a roll-off of 0.15. Within this campaign we observed no significant difference in the total amount of NLI generated when varying this parameter.

A variety of system configurations were tested by varying pairs of symbol rates, R_s, and WDM grid spacings, Δf, which are shown in their entirety in Tab. 1. With the exception of the presently extensively deployed $R_s = 32\,\text{GBd}$, $\Delta f = 50\,\text{GHz}$ spacing scenario, every configuration retains an identical $R_s/\Delta f$ ratio of 0.85 in order to observe the effect of varying the symbol rate. The number of channels in the full spectrum simulation is set to fill approximately 1 THz of the optical spectrum, with the CUT always being the center channel of the WDM comb. The channel launch power is set according to the local-optimization, global-optimization (LOGO) power [36], P_{LOGO}, which is calculated for each symbol rate from the overall optimum PSD by estimating the NLI after one span, η_{NLI}, using the GN model [13]. This choice of number of channels and launch powers ensures a fair comparison of the QoT performance between

OSA CONTINUUM

different symbol rates and frequency spacing schemes. In order to isolate the XPM contribution in the P&P simulation, we set the probe power sufficiently low in order to avoid significant SPM contributions: for pumps far enough away from the probe, (k>1), the probe power is set to −20 dBm; instead, for the pump adjacent to the probe, (k = 1), the probe power is set to the LOGO power attenuated by 4 dB in order to mitigate the linear crosstalk of the pump on the probe as illustrated in Fig. 1(a-b). In the latter case, a small amount of SPM is still present and is removed using the results of a single channel simulation. The fiber propagation is performed by numerically solving the Manakov equation using the SSFM. In this scenario, it is accurate to use the Manakov equation as it has been demonstrated that the polarization mode dispersion (PMD) has a negligible interaction with NLI generation [37], and dual-polarization modulated signals allow to rely on the polarization-average wave equation for fiber propagation [38]. The non-linear step size of the SSFM has been optimized in order to ensure constant accuracy as the simulation bandwidth increases for the individual P&P simulations [39].

Table 1. List of the different spectral configurations used in the simulation campaign. Third column shows the ratio between the symbol rate and WDM grid spacing.

Symbol Rate (GBd)	WDM Grid Spacing (GHz)	Ratio	N_{ch}
32	37.5	0.85	29
32	50	0.64	21
42.5	50	0.85	21
64	72	0.85	15
85	100	0.85	11

The OLS is composed of a sequence of 20 fiber spans, each 80 km long, with a fiber loss coefficient, α_{dB} of 0.18 dB/km and a non-linearity coefficient, γ of 1.27 /W/km. For the dispersion coefficient we have instead tested three values; $D = 2$, 5 and 16.7 ps / (nm·km). These dispersion values show a general picture of the dispersion effect upon the NLI generation for different symbol rates. In this study, we consider uniform OLSs where all fiber spans have an identical set of configurations. Given the principle of spatial disaggregation, each fiber span can be considered separately. Therefore, restricting the simulations to uniform OLSs does not undermine the generality of the presented methodology, meaning that subsequent results can be extended to non-uniform OLS scenarios. Focusing on the $D = 2$ ps / (nm·km) case, these chromatic dispersion values refer to bands ranging from L to E, and part of the O band. Propagation loss is recovered at the end of each span by ideal, flat, noiseless Erbium-doped fiber amplifiers (EDFA)s. For the LOGO power calculation the EDFA noise figure is assumed to be 5 dB. The propagated signal is then processed by the DSP-based receiver. The optical hybrid is considered ideal so that the four quadratures are recovered with no additional impairment. The received signal is then sampled at two samples per symbol and passed through the adaptive equalizer stage which converges to the matched filter. The equalizer uses a least mean squares (LMS) algorithm, with 42 taps and one adaptation coefficient value of $\mu = 10^{-4}$, over the entire observed signal [40]. Noise arising from quantization errors within the analog to digital converter (ADC) and electrical noise are not considered, in order to focus on the NLI measurements.

The signal is subsequently processed by a CPE stage that utilizes the Viterbi-Viterbi algorithm [41], allowing full recovery of the NLPN. In Fig. 2(b), the scattering diagram shows that the CPE algorithm has completely recovered the NLPN, leaving only circular noise on the constellation points. It is worth noting that, for each single P&P simulation there exists an optimal CPE value which may vary slightly with respect to that of the optimal full spectrum simulation, depending upon the system parameters and the spectral distance of the pump from the CUT. As changing the CPE length for each pump within the superposition would produce a result that is not fully

representative of the corresponding full-spectrum simulation, within this work we fix the optimal CPE to be equal to that of the full-spectrum simulation, with an optimized averaging length of 8 symbols for the calculation of any SNR contribution.

4. Spectral disaggregation

In this section we compare the result of the superposition of the individual P&P simulations with those of the full-spectrum simulation through the difference in non-linear SNR between them, defined as:

$$\epsilon_n = \mathrm{SNR}_{\mathrm{Full},n} - \mathrm{SNR}_{\mathrm{Sup},n}\ , \tag{4}$$

where $\mathrm{SNR}_{\mathrm{Full},n}$ and $\mathrm{SNR}_{\mathrm{Sup},n}$ are the $\mathrm{SNR}_{\mathrm{NL}}$ of the full-spectrum and superposition scenarios, respectively, at the end of the n-th fiber span, expressed in dB. Consequently, a positive value of ϵ_n means that the superposition delivers a conservative QoT with respect to the full-spectrum result. In this case, we set $n = N_s$ and compare the $\mathrm{SNR}_{\mathrm{NL}}$ obtained by full-spectrum simulations and superposition after the propagation over $N_s = 20$ spans. In Fig. 3 we show the results

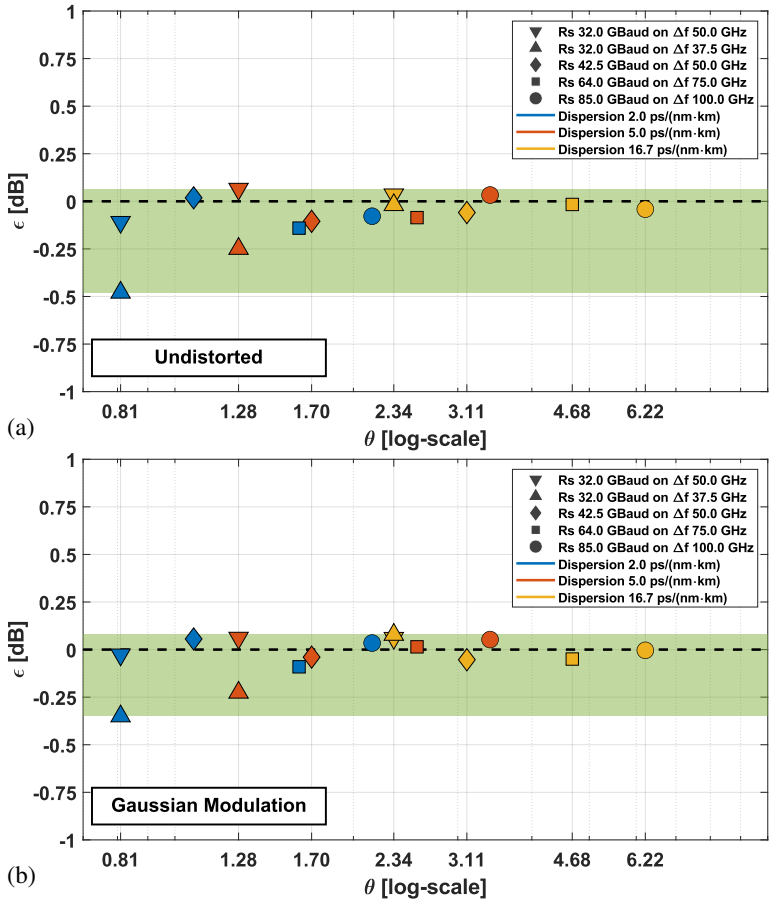

Fig. 3. The error at the last span ϵ_{20} between the superimposed and full-spectrum scenarios assuming spectral disaggregation for all simulation campaign configurations for: (a) PM-QPSK modulated pumps and (b) Gaussian modulated pumps.

OSA CONTINUUM

of this analysis, plotting ϵ_{20} against the parameter $\theta = \pi|\beta_2|LR_s^2$ that fully encloses all NLI-dependent configuration parameters [15]. For all cases analyzed, it is visible that ϵ lies within a 0.5 dB range (area highlighted in green), for both the undistorted and Gaussian modulated transmission scenarios. Furthermore, there exists one extreme case (R_s = 32 GBd, Δf = 37.5 GHz, D = 2 ps / (nm·km)) without which the maximum error would be halved. Moreover, for the case where the dispersion and symbol rate remain identical but the WDM grid spacing is increased (R_s = 32 GBd, Δf = 37.5 GHz and R_s = 32 GBd, Δf = 50 GHz) there is an improvement in the accuracy of the superposition. This is a consequence of simulations with smaller WDM grid spacings generating noisier results, especially in the lowest dispersion case. Furthermore, Fig. 3 shows how an increase of chromatic dispersion for a constant symbol rate and WDM grid spacing improves the accuracy of the superposition with respect to the full-spectrum scenario. These findings are valid for all simulations performed within this work, for both the undistorted and Gaussian modulated pump cases. Remarkably, even for the worst case configuration scenario, Eq. 3 provides an accurate estimation for the total $\mathrm{SNR_{NL}}$ confirming the spectral disaggregation hypothesis.

5. Spatial disaggregation

We now tackle the prospect of spatial disaggregation by considering the SNR span-by-span degradation, $\Delta\mathrm{SNR_{NL}}$, which is the inverse difference in linear power between the $\mathrm{SNR_{NL}}$ at the end of the n-th span and $(n-1)$-th span, converted into dB. In Fig. 4 we present the $\Delta\mathrm{SNR_{NL}}$ introduced by each span for a subset of the configuration scenarios, representing a range of symbol rates, fiber chromatic dispersion values and WDM grid spacings. These figures report

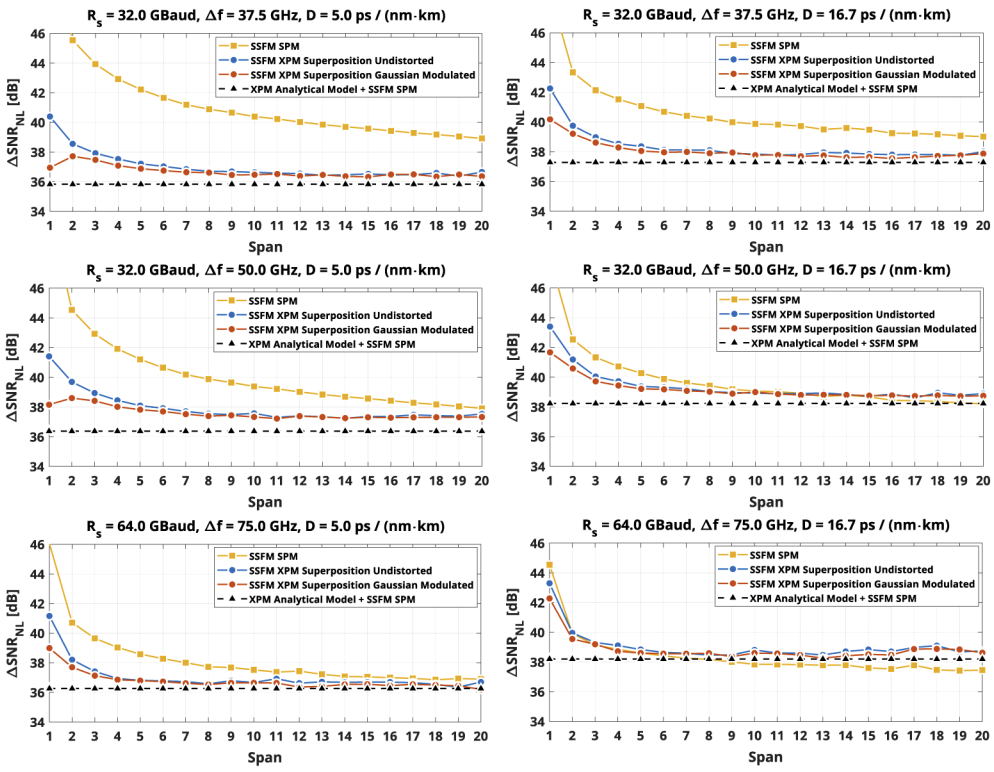

Fig. 4. The non-linear SNR span-by-span increments $\Delta\mathrm{SNR_{NL}}$, for a subset of the overall simulation campaign.

OSA CONTINUUM

the CUT SPM contribution and the total XPM contribution obtained by summing the XPM generated by all pumps, denoted $\Delta\text{SNR}_{\text{SPM}}$ and $\Delta\text{SNR}_{\text{XPM}}$, respectively, for both QPSK and Gaussian-modulated cases. As an additional reference, we include the corresponding estimations obtained with the analytical model of the XPM contribution presented in [14], which produces a conservative SNR prediction in all analyzed scenarios. Within these figures it is visible that the $\Delta\text{SNR}_{\text{XPM}}$ reaches a constant value after a given number of fiber spans, representing a fully incoherent accumulation regime, for all analyzed configuration scenarios. Therefore, we can conclude that, at least for the XPM, spatial disaggregation is achieved, meaning that the corresponding final SNR of an OLS depends only upon the single-span contribution. On the other hand, the $\Delta\text{SNR}_{\text{SPM}}$ continues to decrease towards a non-constant value, representing the statistically coherent accumulation of the SPM through the previously crossed fiber spans.

Following this, the obstacle to a completely spatially disaggregated approach is solely the SPM contribution to the NLI. Nevertheless, as shown in [15], it is possible to estimate a correction coefficient which maximizes the coherency effect and also allows the management of the SPM in a spatially disaggregated approach. In conclusion, it is worth noting that for some configurations, the SPM becomes the leading contribution to the total NLI as a result of this coherent accumulation, such as for the cases where $R_s = 32\,\text{GBd}$, $\Delta f = 50\,\text{GHz}$, $D = 16.7\,\text{ps}/(\text{nm}\cdot\text{km})$ and $R_s = 64\,\text{GBd}$, $\Delta f = 75\,\text{GHz}$ and $D = 16.7\,\text{ps}/(\text{nm}\cdot\text{km})$ in Fig. 4. It can be seen from these examples that the SPM becomes more dominant as the symbol rate is increased, meaning that there is a loss of accuracy when an incoherent model (such as those discussed in Sec. 2) is applied.

6. Predicting SNR in the fully disaggregated approach

As mentioned in the previous section, the simulated XPM values require a given number of spans to reach the constant expected value, as in Fig. 4, with the initial accumulation containing a transient. This transient is present for all P&P scenarios investigated within the simulation campaign and it is reasonable to assume that it is also present for all corresponding full-spectrum scenarios – this is not shown within this work. The result of this effect is that within this transient region the simulation tool demonstrates less accuracy and, as a result, there is a minor reduction in accuracy to the SNR recovered at all subsequent fiber spans. As stated within Sec. 4, the metric of accuracy of the spectral superposition is expressed using Eq. 4 evaluated at the final span, with the results of this approach shown in Fig. 3. These results may be refined by incorporating a compensation for this inaccurate transient contribution. Consequently, we re-scale the accumulations of both the full-spectrum and superposition cases to their respective 10-th span values, where, for all scenarios, a constant value for the $\Delta\text{SNR}_{\text{NL}}$ is reached. The re-scaled span-by-span SNRs for the full-spectrum and superposition cases, $\overline{\text{SNR}}_{\text{Full},n}$, and $\overline{\text{SNR}}_{\text{Sup},n}$, respectively, can hence be expressed as:

$$\overline{\text{SNR}}_{\text{Full},n} = \left(\text{SNR}^{-1}_{\text{Full},n} - \text{SNR}^{-1}_{\text{Full},10}\right)^{-1}, \tag{5}$$

$$\overline{\text{SNR}}_{\text{Sup},n} = \left(\text{SNR}^{-1}_{\text{Sup},n} - \text{SNR}^{-1}_{\text{Sup},10}\right)^{-1}. \tag{6}$$

In Fig. 5 we show the results obtained by evaluating Eq. 4 considering Eq. 5 and Eq. 6. Although not always conservative, these plots demonstrate that the recovery of the full-spectrum results using the superposition method reaches an even higher level of accuracy with respect to Fig. 3, with a maximum non-conservative error of -0.2 dB for $R_s = 32\,\text{GBd}$, $\Delta f = 37.5\,\text{GHz}$, $D = 2\,\text{ps}/(\text{nm}\cdot\text{km})$.

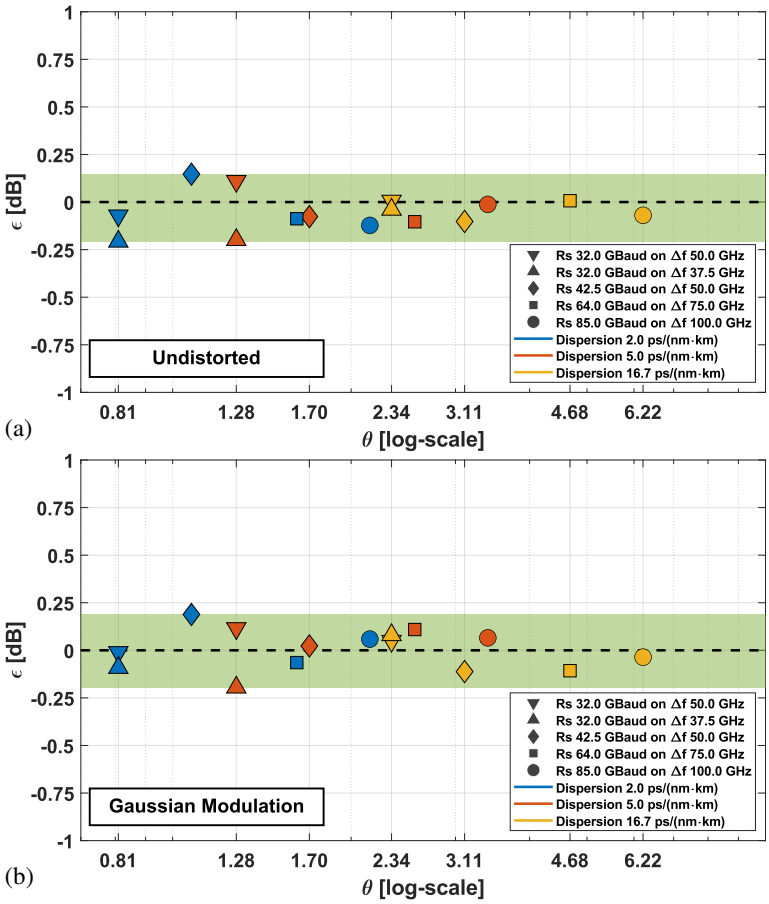

Fig. 5. The error at the last span ϵ_{20} between the superimposed and full-spectrum scenarios, re-scaled to compensate for the inherent transient, for all simulation campaign configurations for: (a) PM-QPSK modulated pumps and (b) Gaussian modulated pumps.

7. Conclusions

In this paper we have demonstrated through an extensive SSFM simulation campaign that the NLI generated by WDM channels co-propagating with a given CUT (the XC-NLI caused by XPM) can be considered as spectrally and spatially generated for a wide range of scenarios, including most practical deployed OLSs. Subsequently, each fiber span as well as the effect of each channel per span can be assumed to provide an independent contribution to the overall NLI that is accumulated over a transparent LP and considered on an individual basis. Given the investigated set of parameters, we can say that the approach is valid for most commercial fibers that operate on the C-band and, additionally, for multi-band OLSs that utilize ITU-T G.652D fiber on the L to E bands and partially on the O-band. While the SC-NLI can be spectrally disaggregated, it is affected by a spatially statistical coherency, meaning that a fully disaggregated management strategy must be based upon an upper-bound. We also note that by increasing symbol rates and narrowing channel spacings the SC-NLI becomes the dominant contribution to the total NLI, highlighting that in ultra-high symbol rate OLSs the coherent accumulation of the SC-NLI must be accurately accounted for. In conclusion, we show in this work that it is possible to produce a conservative, fully disaggregated physical layer model of an optical network.

OSA CONTINUUM

Funding

H2020 Marie Skłodowska-Curie Actions (814276).

Disclosures

The authors declare no conflicts of interest.

References

1. Cisco, "Cisco visual networking index: Forecast and methodology," https://www.cisco.com/c/en/us/solutions/service-provider/visual-networking-index-vni/index.html (2018). [Online; accessed 8-September-2020].
2. H. Sun, M. Torbatian, M. Karimi, R. Maher, S. Thomson, M. Tehrani, Y. Gao, A. Kumpera, G. Soliman, A. Kakkar, M. Osman, Z. A. El-Sahn, C. Doggart, W. Hou, S. Sutarwala, Y. Wu, M. R. Chitgarha, V. Lal, H.-S. Tsai, S. Corzine, J. Zhang, J. Osenbach, S. Buggaveeti, Z. Morbi, M. I. Olmedo, I. Leung, X. Xu, P. Samra, V. Dominic, S. Sanders, M. Ziari, A. Napoli, B. Spinnler, K.-T. Wu, and P. Kandappan, "800G DSP ASIC design using probabilistic shaping and digital sub-carrier multiplexing," J. Lightwave Technol. **38**(17), 4744–4756 (2020).
3. B. Varghese and R. Buyya, "Next generation cloud computing: New trends and research directions," Futur. Gener. Comput. Syst. **79**, 849–861 (2018).
4. A. Ferrari, A. Napoli, J. K. Fischer, N. M. S. da Costa, A. D'Amico, J. Pedro, W. Forysiak, E. Pincemin, A. Lord, A. Stavdas, J. P. F.-P. Gimenez, G. Roelkens, N. Calabretta, S. Abrate, B. Sommerkorn-Krombholz, and V. Curri, "Assessment on the achievable throughput of multi-band ITU-T G. 652. D fiber transmission systems," J. Lightwave Technol. **38**(16), 4279–4291 (2020).
5. Cisco, "Cisco Visual Networking Index: Forecast and Trends, 2017–2022", Tech. rep., Cisco (2017).
6. P. Sarigiannidis, T. Lagkas, S. Bibi, A. Ampatzoglou, and P. Bellavista, "Hybrid 5g optical-wireless sdn-based networks, challenges and open issues," IET Networks **6**(6), 141–148 (2017).
7. F. Boccardi, R. W. Heath, A. Lozano, T. L. Marzetta, and P. Popovski, "Five disruptive technology directions for 5g," IEEE Commun. Mag. **52**(2), 74–80 (2014).
8. K. Roberts, Q. Zhuge, I. Monga, S. Gareau, and C. Laperle, "Beyond 100 gb/s: capacity, flexibility, and network optimization," J. Opt. Commun. Netw. **9**(4), C12–C23 (2017).
9. N. Sambo, P. Castoldi, A. D'Errico, E. Riccardi, A. Pagano, M. S. Moreolo, J. M. Fàbrega, D. Rafique, A. Napoli, S. Frigerio, E. H. Salas, G. Zervas, M. Nölle, J. K. Fischer, A. Lord, and J. P. F.-P. Gimenez, "Next generation sliceable bandwidth variable transponders," IEEE Commun. Mag. **53**(2), 163–171 (2015).
10. M. Gunkel, A. Mattheus, F. Wissel, A. Napoli, J. Pedro, N. Costa, T. Rahman, G. Meloni, F. Fresi, F. Cugini, N. Sambo, and M. Bohn, "Vendor-interoperable elastic optical interfaces: Standards, experiments, and challenges," J. Opt. Commun. Netw. **7**(12), B184–B193 (2015).
11. M. Filer, H. Chaouch, and X. Wu, "Toward transport ecosystem interoperability enabled by vendor-diverse coherent optical sources over an open line system," J. Opt. Commun. Netw. **10**(2), A216–A224 (2018).
12. J.-L. Auge, G. Grammel, E. Le Rouzic, V. Curri, G. Galimberti, and J. Powell, "Open optical network planning demonstration," in *Optical Fiber Communication Conference*, (Optical Society of America, 2019), pp. M3Z–9.
13. A. Carena, G. Bosco, V. Curri, P. Poggiolini, and F. Forghieri, "Impact of the transmitted signal initial dispersion transient on the accuracy of the GN-model of non-linear propagation," in *39th European Conference and Exhibition on Optical Communication (ECOC 2013)*, (IET, 2013), pp. 1–3.
14. E. Virgillito, A. D'Amico, A. Ferrari, and V. Curri, "Observing and modeling wideband generation of non-linear interference," in *2019 21st International Conference on Transparent Optical Networks (ICTON)*, (IEEE, 2019), pp. 1–4.
15. A. D'Amico, E. London, E. Virgillito, A. Napoli, and V. Curri, "Quality of transmission estimation for planning of disaggregated optical networks," in *2020 International Conference on Optical Network Design and Modeling (ONDM)*, (2020), pp. 1–3.
16. A. Carena, V. Curri, G. Bosco, P. Poggiolini, and F. Forghieri, "Modeling of the impact of nonlinear propagation effects in uncompensated optical coherent transmission links," J. Lightwave Technol. **30**(10), 1524–1539 (2012).
17. P. Johannisson and M. Karlsson, "Perturbation analysis of nonlinear propagation in a strongly dispersive optical communication system," J. Lightwave Technol. **31**(8), 1273–1282 (2013).
18. V. Oliari, E. Agrell, and A. Alvarado, "Regular perturbation on the group-velocity dispersion parameter for nonlinear fibre-optical communications," Nat. Commun. **11**(1), 933 (2020).
19. A. Bononi, P. Serena, N. Rossi, E. Grellier, and F. Vacondio, "Modeling nonlinearity in coherent transmissions with dominant intrachannel-four-wave-mixing," Opt. Express **20**(7), 7777–7791 (2012).
20. A. Mecozzi and R.-J. Essiambre, "Nonlinear shannon limit in pseudolinear coherent systems," J. Lightwave Technol. **30**(12), 2011–2024 (2012).
21. M. Secondini and E. Forestieri, "Analytical fiber-optic channel model in the presence of cross-phase modulation," IEEE Photonics Technol. Lett. **24**(22), 2016–2019 (2012).
22. R. Dar, M. Feder, A. Mecozzi, and M. Shtaif, "Pulse collision picture of inter-channel nonlinear interference in fiber-optic communications," J. Lightwave Technol. **34**(2), 593–607 (2016).

OSA CONTINUUM

23. V. Curri, A. Carena, P. Poggiolini, G. Bosco, and F. Forghieri, "Extension and validation of the GN model for non-linear interference to uncompensated links using Raman amplification," Opt. Express **21**(3), 3308–3317 (2013).
24. M. Cantono, D. Pilori, A. Ferrari, C. Catanese, J. Thouras, J.-L. Augé, and V. Curri, "On the interplay of nonlinear interference generation with stimulated raman scattering for QoT estimation," J. Lightwave Technol. **36**(15), 3131–3141 (2018).
25. A. Carena, G. Bosco, V. Curri, Y. Jiang, P. Poggiolini, and F. Forghieri, "EGN model of non-linear fiber propagation," Opt. Express **22**(13), 16335–16362 (2014).
26. A. Nespola, S. Straullu, A. Carena, G. Bosco, R. Cigliutti, V. Curri, P. Poggiolini, M. Hirano, Y. Yamamoto, T. Sasaki, J. Bauwelinck, K. Verheyen, and F. Forghieri, "GN-model validation over seven fiber types in uncompensated PM-16QAM Nyquist-WDM links," IEEE Photonics Technol. Lett. **26**(2), 206–209 (2014).
27. M. Filer, M. Cantono, A. Ferrari, G. Grammel, G. Galimberti, and V. Curri, "Multi-Vendor Experimental Validation of an Open Source QoT Estimator for Optical Networks," J. Lightwave Technol. **36**(15), 3073–3082 (2018).
28. V. Curri, "Software-defined WDM optical transport in disaggregated open optical networks", in *ICTON 2020,* (2020), p. We.C2.1.
29. R. Dar, M. Feder, A. Mecozzi, and M. Shtaif, "Properties of nonlinear noise in long, dispersion-uncompensated fiber links," Opt. Express **21**(22), 25685–25699 (2013).
30. S. M. Bilal, C. R. Fludger, V. Curri, and G. Bosco, "Multistage carrier phase estimation algorithms for phase noise mitigation in 64-quadrature amplitude modulation optical systems," J. Lightwave Technol. **32**(17), 2973–2980 (2014).
31. S. J. Savory, G. Gavioli, R. I. Killey, and P. Bayvel, "Electronic compensation of chromatic dispersion using a digital coherent receiver," Opt. Express **15**(5), 2120–2126 (2007).
32. A. Ferrari, M. Filer, K. Balasubramanian, Y. Yin, E. L. Rouzic, J. Kundrát, G. Grammel, G. Galimberti, and V. Curri, "GNPy: an open source application for physical layer aware open optical networks," J. Opt. Commun. Netw. **12**(6), C31–C40 (2020).
33. D. J. Ives, P. Bayvel, and S. J. Savory, "Adapting transmitter power and modulation format to improve optical network performance utilizing the Gaussian noise model of nonlinear impairments," J. Lightwave Technol. **32**(21), 4087–4096 (2014).
34. D. Pilori, M. Cantono, A. Carena, and V. Curri, "FFSS: The fast fiber simulator software," in *2017 19th International Conference on Transparent Optical Networks (ICTON)*, (2017), pp. 1–4.
35. A. Carena, G. Bosco, V. Curri, P. Poggiolini, M. T. Taiba, and F. Forghieri, "Statistical characterization of PM-QPSK signals after propagation in uncompensated fiber links," in *36th European Conference and Exhibition on Optical Communication*, (IEEE, 2010), pp. 1–3.
36. R. Pastorelli, S. Piciaccia, G. Galimberti, E. Self, M. Brunella, G. Calabretta, F. Forghieri, D. Siracusa, A. Zanardi, E. Salvadori, G. Bosco, A. Carena, V. Curri, and P. Poggiolini, "Optical control plane based on an analytical model of non-linear transmission effects in a self-optimized network," in *39th European Conference and Exhibition on Optical Communication (ECOC 2013)*, (2013), pp. 1–3.
37. M. Cantono, D. Pilori, A. Ferrari, A. Carena, and V. Curri, "Observing the interaction of PMD with generation of NLI in uncompensated amplified optical links," in *2018 Optical Fiber Communications Conference and Exposition (OFC)*, (2018), pp. 1–3.
38. D. Marcuse, C. R. Manyuk, and P. K. A. Wai, "Application of the manakov-pmd equation to studies of signal propagation in optical fibers with randomly varying birefringence," J. Lightwave Technol. **15**(9), 1735–1746 (1997).
39. S. Musetti, P. Serena, and A. Bononi, "On the accuracy of split-step Fourier simulations for wideband nonlinear optical communications," J. Lightwave Technol. **36**(23), 5669–5677 (2018).
40. J. R. Barry, E. A. Lee, and D. G. Messerschmitt, *Digital communication* (Springer Science & Business Media, 2012).
41. A. Viterbi, "Nonlinear estimation of PSK-modulated carrier phase with application to burst digital transmission," IEEE Trans. Inf. Theory **29**(4), 543–551 (1983).